Letter

Tunable sigmoid behavior of a magnon-based parametron using a $Y_3Fe_5O_{12}$/Pt bilayer disk

Geil Emdi,[1] Tomosato Hioki,[1,2,3,*] Takahiko Makiuchi,[1,3] and Eiji Saitoh[1,2,3,4,5]

[1] *Department of Applied Physics, The University of Tokyo, Tokyo 113-8656, Japan*
[2] *Advanced Institute for Materials Research, Tohoku University, Sendai 980-857, Japan*
[3] *RIKEN Center for Emergent Matter Science (CEMS), Wako 351-0198, Japan*
[4] *Institute for AI and Beyond, The University of Tokyo, Tokyo 113-8656, Japan*
[5] *Advanced Science Research Center, Japan Atomic Energy Agency, Tokai 319-1195, Japan*

(Received 18 March 2024; revised 23 June 2024; accepted 13 August 2024; published 9 September 2024)

Sigmoidal curve behavior of 0 and π state probability in a magnon parametron, using yttrium iron garnet ($Y_3Fe_5O_{12}$) thin disk, is systematically investigated. We demonstrate that the probability distribution can be tuned by bias and pump microwave power. Our numerical calculation that considers increasing damping due to four-magnon scattering processes reproduces the results well.

DOI: 10.1103/PhysRevApplied.22.L031002

Nonlinear activation function is a key element in a neural network, which is capable of approximating any continuous function [1]. The activation function exhibits a sigmoidlike curve against input, and its steepness is widely used for optimization of neural networks for better inference quality [2]. Owing to their versatility, neural networks are widely used for various complex tasks [3,4]. In general, the nonlinear activation function is realized in CMOS-based devices, which require many logic bits for emulating such nonlinear and continuous responses [4–7], whereas it can be realized by a single physical entity with strong nonlinearity.

In magnetic materials, collective precessional motion of spins propagates as waves, known as spin waves, with their elementary excitations termed magnons. The interactions between magnons are governed by dipolar and exchange interactions, leading to strong nonlinearity of their dynamics [8,9]. Parametric excitation is one example of nonlinear processes, where magnons with half of the microwave frequency are excited and randomly exhibit two degenerate stable phases, 0 and π [10–14]. With the application of an auxiliary microwave field with the magnon frequency, the occurrence of either phase state can be biased, leading to nonlinear response of the mean magnon amplitude [12,15].

Here, we present sigmoid curve behavior of a magnon parametron tuned by auxiliary microwaves with the ferromagnetic resonance frequency. We find that the steepness of the sigmoidlike curve depends on the pump power applied due to magnon-magnon scatterings in the system. Our model calculation based on the Fokker-Planck equation for magnon dynamics reproduces the experimental results well.

We use an yttrium iron garnet ($Y_3Fe_5O_{12}$; YIG) microsized thin disk that is covered with a platinum (Pt) thin layer as shown in Fig. 1(a). The diameter of the YIG disk is 200 μm and the thickness is 370 nm. We deposit the YIG layer on top of a gadolinium gallium garnet substrate by magnetron sputtering and annealing. Then, a 10-nm-thick Pt film is sputtered on top of the YIG layer. The disk shape of the YIG/Pt bilayer is patterned by photolithography and Ar-ion milling processes. Moreover, two gold electrodes are sputtered at the edge of the Pt film. The fabricated sample is placed on top of a main coplanar waveguide (CPW) that is short-ended, with a width of 200 μm. One of the gold electrodes is grounded, while the other is connected to a secondary CPW [see Fig. 1(a)].

We generate the rf pump field, $\mathbf{h}_{2f}$, through the main CPW at twice the resonant frequency of $2f = 4.3$ GHz, parallel to the static field. Owing to the nonlinearity and fluctuations in the magnet, the pump field will parametrically excite the magnetization precession with a randomly selected initial phase of 0 or π relative to the pump field [see Fig. 1(b)]. In addition, we generate the rf bias field, $\mathbf{h}_b$, through the main CPW at a frequency of $1f = 2.15$ GHz. We use the stray component of $\mathbf{h}_b$, perpendicular to the static field, to control the occurrence probability of 0 and π states. The bias field intensity is estimated by Ampere's law [8]: $h_b \approx (1/2w)\sqrt{P_b/Z}$, where P_b is the bias microwave power, $w = 200$ μm is the width of the CPW, and $Z = 50\ \Omega$ is the characteristic impedance of the CPW. The bias field is modulated into a 40-μs-width pulse and the pump field is shaped into a pulse of 20 μs width. We set the pulse rise time of the bias field

*Contact author: tomosato.hioki@ap.t.u-tokyo.ac.jp

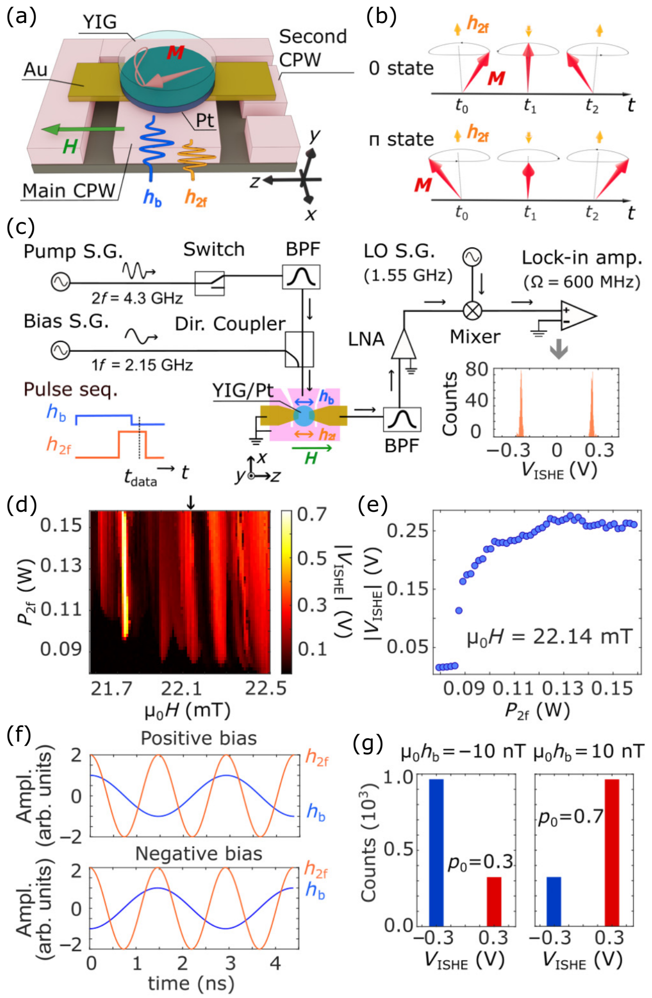

FIG. 1. (a) Schematic setup of the of YIG/Pt bilayer sample and coplanar waveguide configuration. **H** is the static magnetic field, $\mathbf{h}_{2f}$ is the ac pump field at twice the FMR frequency, and $\mathbf{h}_b$ is the ac bias field at the FMR frequency. Note that we use the stray transverse component of $\mathbf{h}_b$ to perform the biasing. (b) Schematic illustration of the 0 and π state magnetization precession in the time domain. (c) Schematic setup of microwave circuit diagram and the pulse timings. All of the signal generators and the lock-in amplifier are synchronized with a 10-MHz rubidium standard. The inset shows the density distribution of the detected ISHE voltages. (d) Pump power and magnetic field dependence of the ISHE voltages due to parametric excitation. (e) ISHE voltage dependence on pump power at $\mu_0 H = 22.14$ mT. (f) Schematic illustrations of the pump and bias microwaves for positive and negative bias field. (g) Occurrence probability of 0 and π states at bias amplitude with opposite phases (π phase difference) at $\mu_0 H = 22.14$ mT and $P_{2f} = 0.125$ W.

to be 30 μs before the rise time of the pump field [see Fig. 1(c)]. By applying the bias field at the start of parametric excitation, we can drive the initial magnetization precession at a fixed phase relative to the bias field by ferromagnetic resonance (FMR). This initial precession acts as a “seed”, which determines the occurrence of 0 or π state. The resulting magnetization precession is detected via ac spin pumping and the inverse spin Hall effect (ISHE) [16–27] as the ac voltage signal transmitted through the secondary CPW. This signal is sent through a mixer, which multiplies the signal at $1f = 2.15$ GHz with a 1.55-GHz waveform generated by a local oscillator (LO). The ac signal is thus down-converted to 600 MHz and it is measured by a megahertz lock-in amplifier (UHFLI, Zurich Instruments) with a lock-in frequency of 600 MHz [Fig. 1(c)]. We record the data at 6 μs after the fall time of the bias pulse, indicated by t_{data} in Fig. 1(c). We repeat the ISHE voltage measurement over 1000 times and we obtain the frequency histogram—hereafter called “counts”—of the detected ISHE voltages [Fig. 1(c) inset].

To find the conditions for parametric excitation, we perform a systematic measurement of the ISHE voltages as a function of static magnetic field and pump power as shown in Fig. 1(d). Above the power thresholds, there are multiple peak structures corresponding to the different standing spin wave modes, which are excited by parametric pumping [28]. We conduct the experiments at $\mu_0 H = 22.14$ mT, indicated by the black arrow in Fig. 1(d), and we show the ISHE voltages as a function of pump power in Fig. 1(e).

The occurrence probability of the 0 state is defined to be $p_0 = \int_{0\,\mathrm{V}}^{0.8\,\mathrm{V}} F(V_{\mathrm{ISHE}})\, dV_{\mathrm{ISHE}}$, where $F(V_{\mathrm{ISHE}})$ is the distribution density normalized such that $\int F(V_{\mathrm{ISHE}})\, dV_{\mathrm{ISHE}} = 1$. The occurrence probability of the π state is $p_\pi = \int_{-0.8\,\mathrm{V}}^{0\,\mathrm{V}} F(V_{\mathrm{ISHE}})\, dV_{\mathrm{ISHE}}$. Firstly, we measure p_0 by changing the bias microwave phase (see Supplemental Material [29]) at $P = 0.089$ and 0.125 W and determine the phase where p_0 takes maximum (minimum) for positive (negative) bias microwave field sign. Then, we measure p_0 for every pumping power. Here, we consider the distribution with the peak at positive (negative) ISHE voltage to be the 0 (π) state. In the absence of bias, the 0 and π states occur randomly leading to almost equal probabilities. However, by applying the bias field, we can tune the occurrence probability of the states by varying the bias amplitude ($\mu_0 h_b$). The bias field has a form of $h_b(t) = h_b \cos(2\pi f t + \varphi_b)$, where φ_b is the phase difference between h_{2f} and h_b. We consider the bias field to be positive at $\varphi_b = 0$ and negative at $\varphi_b = \pi$ [see Fig. 1(f)]. In Fig. 1(g), we plot bar graphs of p_0 and p_π. At $\mu_0 h_b = -10$ nT, the 0 state probability is $p_0 = 0.3$. Reversing the bias to be at $\mu_0 h_b = 10$ nT, the probability becomes $p_0 = 0.7$.

In Fig. 2(a), we show the systematic measurement of p_0 as a function of pump power and bias field. The measurement is taken above the pump threshold ($P_{2f} \geq 0.089$ W). We show that the dependence of p_0 is monotonically increasing as a function of $\mu_0 h_b$. As we increase the pump power, the rate at which p_0 rises with $\mu_0 h_b$ decreases. In Fig. 2(b), we show the dependence of p_0 on the bias field, $\mu_0 h_b$, at different pump power. p_0 increases and saturates to $p_0 = 1$ as we increase $\mu_0 h_b$. Conversely, by reversing the bias field to negative value, p_0 decreases and approaches

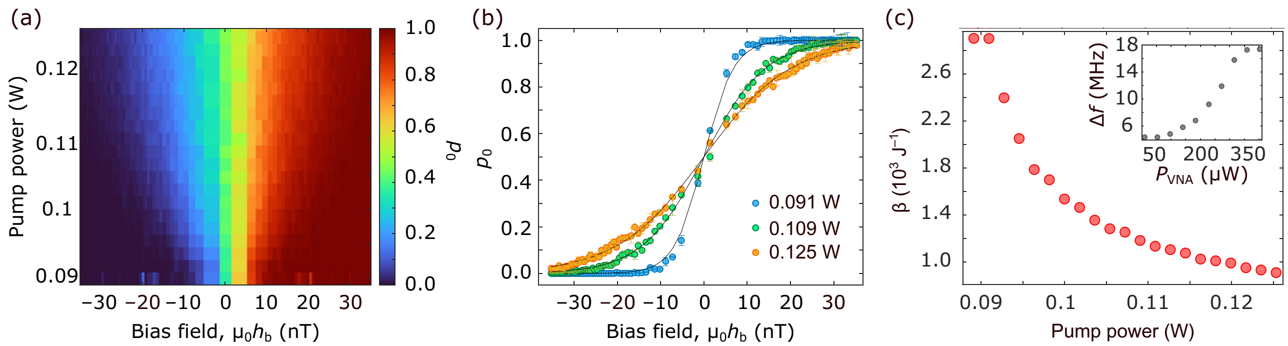

FIG. 2. (a) Heatmap of p_0 as a function pump power and bias fields at $\mu_0 H = 22.14$ mT. (b) Dependence of p_0 on bias fields at different pump power. The black curves show the fitting with sigmoid function: $p_0 = \left(e^{-\beta\mu_0 h_b M_s} + 1\right)^{-1}$, where $\beta = 1/k_B T$. (c) Dependence of β on pump power.

$p_0 = 0$. Thus, the p_0 dependence on $\mu_0 h_b$ has a characteristic of a sigmoid curve, indicative of the nonlinear response of the 0 and π state probability to the bias field. Considering the sigmoid curve behavior at different pump power, we find that the steepness of the sigmoid curves becomes smaller at larger pump power.

We evaluate the steepness of the curves at varying pump power by fitting the $\mu_0 h_b$ dependence data with sigmoid function: $p_0 = \left(e^{-\beta\mu_0 h_b M_s} + 1\right)^{-1}$, where $\beta = 1/k_B T$ and T is the effective temperature. The saturation magnetization is $\mu_0 M_s = 150$ mT. In Fig. 2(c), we plot β as a function of pump power. With increasing pump power, β generally decreases. This shows that the response of the state occurrence probability to the bias field becomes more gradual as pump power rises.

To explain this result, we measure the frequency linewidth of the sample's absorption spectrum using a vector network analyzer (VNA) at varying power P_{VNA} (see Supplemental Material [29]) at $\mu_0 H = 21.7$ mT, where the fundamental FMR mode is excited. The inset of Fig. 2(c) shows the frequency linewidth, Δf, as a function of P_{VNA}. With increasing power, the linewidth rises indicating that the damping in the sample increases with power. Since the standing spin wave mode appearing at $\mu_0 H = 22.14$ mT has weak coupling to the main CPW, we cannot perform linewidth measurement at the field. The increase in damping at strong microwave power might be due to multimagnon scattering processes. When strong microwave power is applied, larger numbers of magnons are excited, leading to a higher rate of scatterings between different magnon modes, such as the second-order Suhl instability [8,30,31], which adds another dissipation channel for the excited magnons. This explanation can also be applied in the case of parametric excitation [13,28], where magnon number rises with increasing pump power.

In addition, increasing damping also implies that there is a larger fluctuation in the magnon system [32–34]. Assuming that the 0 and π states develop instantaneously upon being driven by the pump field, the occurrence probability, p_0, is solely determined by the fluctuations of the magnetization dynamics in the sample. Similarly, the response of the initial magnetization to the bias field is also dependent on the fluctuation, or damping. Thus, we infer that the decrease of β at higher pump power is attributed to the increasing damping in the sample.

To illustrate our discussion, we consider a system of parametric oscillators under dissipation to thermal baths. In a parametric oscillator, a pump field will generate a photon, which splits into two magnons at half of the photon's frequency [8,35–41]. To start off, the Hamiltonian is expressed as [13,32,42]

$$\hat{H} = \hat{H}_0 + \hat{H}_{pump} + \hat{H}_{int} + \hat{H}_{bias} + \hat{H}_{bath}, \tag{1}$$

where $\hat{H}_0$ is the Hamiltonian describing the harmonic oscillator system, written as $\hat{H}_0 = \hbar\omega_p \hat{a}^\dagger \hat{a} + \hbar\omega \hat{c}^\dagger \hat{c}$, where $\hat{a}$ ($\hat{a}^\dagger$) is the annihilation (creation) operator of pump photon and ω_p is the pump frequency. $\hat{c}$ ($\hat{c}^\dagger$) is the annihilation (creation) operator of the magnon with frequency $\omega = 2\pi f$ (after diagonalization of the quadratic terms in the dipolar interaction Hamiltonian [8]). Here, $\omega_p = 2\omega$. $\hat{H}_{pump}$ represents the driving pump fields in generating the pump photons. It is written as

$$\hat{H}_{pump} = i\hbar\left(\varepsilon_p e^{-i(\omega_p t)}\hat{a}^\dagger - \varepsilon_p^* e^{i(\omega_p t)}\hat{a}\right), \tag{2}$$

where ε_p is the amplitude of the classical pump field, $\varepsilon_p = \gamma|h_{2f}|$. $\hat{H}_{int}$ describes the parametric interaction between the driving pump field and the pair of magnons. It is written as

$$\hat{H}_{int} = \frac{i\hbar}{2}\rho_k\left(\hat{c}^\dagger\hat{c}^\dagger\hat{a} - \hat{c}\hat{c}\hat{a}^\dagger\right), \tag{3}$$

where the coupling parameter between the pump photon and magnon is $\rho_k = \omega_M/4\sqrt{\omega_M/\omega}\sin^2\theta_k e^{-i2\varphi_k}$; we use $\omega_M = \gamma\mu_0 M_s$, where γ is the gyromagnetic ratio and θ_k and φ_k are the polar and azimuthal angles of the wave vector, $\mathbf{k}$ [8]. $\hat{H}_{\text{bias}}$ represents the classical bias fields in generating the initial magnetization precession. It is written as

$$\hat{H}_{\text{bias}} = i\hbar\left(\varepsilon_{\text{b}} e^{-i\omega t}\hat{c}^{\dagger} - \varepsilon_{\text{b}}^{*} e^{i\omega t}\hat{c}\right), \tag{4}$$

where ε_{b} is the amplitude of the classical pump field, $\varepsilon_{\text{b}} = \gamma h_{\text{b}}$. Lastly the damping of photon and magnons to the phonon bath is assumed to be written as

$$\hat{H}_{\text{bath}} = \hat{c}\hat{\Gamma}_1^{\dagger} + \hat{c}^{\dagger}\hat{\Gamma}_1 + \hat{a}\hat{\Gamma}_2^{\dagger} + \hat{a}^{\dagger}\hat{\Gamma}_2, \tag{5}$$

where $\hat{\Gamma}_i$ $\left(\hat{\Gamma}_i^{\dagger}\right)$ with $i = 1, 2$ are the annihilation (creation) operators of the harmonic oscillator in the thermal bath of phonons.

Assuming that the damping rate of the pump photon is much larger than that of the magnon mode, we can simplify the analysis by considering only the magnon mode [32,42]. Here, we consider the coherent state of magnon mode $|c\rangle$ with eigenvalue α, such that $\hat{c}\,|c\rangle = \alpha\,|c\rangle$. Separating the real and imaginary components, we write $\alpha = x + ip$. In the rotating frame of $\omega = \omega_{\text{p}}/2$, the Fokker-Planck equation follows [13,42] (see Supplemental Material [29]):

$$\frac{\partial W}{\partial t} = \left\{ \frac{\partial}{\partial \alpha}\left[\alpha - \alpha^{*}\left(\frac{\rho_k \varepsilon_{\text{p}}}{\gamma_0\gamma_2} - \frac{\gamma_{\text{NL}}}{\gamma_0}\alpha^2\right) - \frac{\varepsilon_{\text{b}}}{\gamma_0}\right] + \frac{1+2n_{\text{th}}}{2}\frac{\partial}{\partial\alpha\alpha^{*}}\left(1 + \frac{\gamma_{\text{NL}}}{\gamma_0}|\alpha|^2\right) + \text{H.c.}\right\} W, \tag{6}$$

where γ_0 and γ_2 are the damping rates for magnon and photon modes into the thermal baths, $\gamma_{\text{NL}} = |\rho_k|^2/2\gamma_2$ is the nonlinear damping constant, and $n_{\text{th}} = \left(e^{\hbar\omega_0/k_{\text{B}}T_{\text{s}}} - 1\right)^{-1}$ is the Planck distribution at sample temperature T_{s}.

For simplicity, we consider real solutions for α, such that $\alpha = x$. We assume a solution in the form of $W = N\exp[-\phi(x)]$, where N is the normalizing term and $\phi(x)$ is the potential. In steady states, we have

$$\phi(x) = \frac{1}{(1+2n_{\text{th}})}\left[x^2 - \frac{r}{2\gamma_{\text{NL}}}\ln\left(1 + 2\gamma_{\text{NL}}x^2\right) - \frac{\varepsilon_{\text{b}}}{2\sqrt{\gamma_0\gamma_{\text{NL}}}}\tan^{-1}\left(2\sqrt{\frac{\gamma_{\text{NL}}}{\gamma_0}}x\right)\right], \tag{7}$$

where $r = (\rho_{\text{k}}\varepsilon_{\text{p}}/\gamma_2) - (\gamma_0/2) - \gamma_{\text{NL}}\,(1 + 2n_{\text{th}})$. The last term of the potential corresponds to the effective contribution of the bias field.

In Fig. 3(a), we show the potential at different bias fields. At $\varepsilon_{\text{b}} = 0$, ϕ is a double-well potential with two degenerate minima at $x_{\text{min}} = \pm\sqrt{r/\gamma_{\text{NL}}}$ and a saddle point at $x_{\text{saddle}} = 0$ (green curve). These two minimum points correspond to the 0 and π stable states; and their amplitudes, $|x_{\text{min}}|$, correspond to the magnon amplitude. When a bias field, ε_{b}, is applied into the system, the double-well potential becomes tilted and the tilt's direction depends on the sign of the bias field as shown in Fig. 3(a). This lifts the degeneracy of the two states and the magnons preferably develop into one of the two states: 0 (red curve) or π (blue curve).

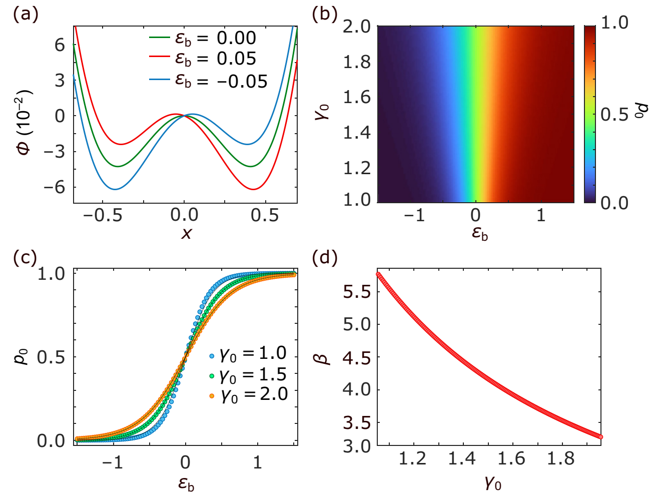

FIG. 3. Numerical results. (a) Potential $\phi(x)$ for different bias fields, ε_{b}. (b) Heatmap of p_0 as a function of damping, γ_0, and bias field, ε_{b}. (c) p_0 as a function bias field at different γ_0. The black curves are the fitting curve: $p_0 = \left(e^{-\beta\varepsilon_{\text{b}}} + 1\right)^{-1}$. (d) β as a function of linear damping, γ_0.

Using this potential solution, we numerically calculate the 0-state occurrence probability defined as

$$p_0 = \int_0^{\infty} W(x)\,dx. \tag{8}$$

We simulate the model by considering thermal magnon number $n_{\text{th}} = 1$ and nonlinear damping constant $\gamma_{\text{NL}} = 0.4$. We compute the dependence of p_0 as a function of damping, γ_0, and bias amplitude, ε_{b}, as shown in Fig. 3(b). As shown in Fig. 3(c), the shape of p_0 as a function of ε_{b} follows a sigmoid curve. Moreover, the sigmoid steepness falls as the damping, γ_0, becomes larger. We evaluate this steepness by fitting the sigmoid curves at varying pump amplitude with sigmoid function: $p_0 = \left(e^{-\beta\varepsilon_{\text{b}}} + 1\right)^{-1}$, where β represents the steepness of the sigmoid curves. As shown in Fig. 3(d), β generally falls with increasing γ_0, which is in agreement with our experimental results and the above discussion. This decrease in β is attributed to the increasing linear damping constant, γ_0, leading to the decreasing effective bias term in the potential, which is proportional to $\varepsilon_{\text{b}}/\sqrt{\gamma_0\gamma_{\text{NL}}}$ [Eq. (7)].

We also consider the possibility of increasing γ_{NL}. The nonlinear damping constant is only dependent on the parametric coupling, ρ_{k}, and the photon damping rate, γ_2. Neither parameter, however, is dependent on pump amplitude; thus the effect of γ_{NL} on β can be disregarded. Additionally, we consider the effect from sample temperature increase. In the limit of $\hbar\omega \ll k_B T_s$, $n_{\mathrm{th}} \propto T_s$ and, thus, $\beta \propto 1/T_s$. From the experimental result [Fig. 2(c)], β decreases by a factor of approximately 3, implying that the sample temperature rises by 3 times room temperature. The final sample temperature considered here is not practical in our experiment. Hence, we can eliminate the effects of increasing both γ_{NL} and T_s on β.

Another possible explanation is the increasing phase shift between h_b and the excited 0 or π phase state owing to nonlinearity at higher pump power. When strong pumping power is applied to the sample, owing to the Kerr-type nonlinearity in magnons, a frequency shift is induced. This manifests itself as the shift in the peak position in Fig. 1(d) with increasing pumping power. When the phase shift appears, the final 0 state has slightly different phase from the 0 state excited by the bias microwave. Therefore, if p_0 is defined by using the 0 state with respect to bias microwave, p_0 will be affected by the nonlinear phase shift. To exclude the artifact from this nonlinear shift, we employ the bias-phase dependence measurement so that the 0 state for defining p_0 is defined with respect not to the bias microwave phase, but to the excited oscillation phase. As a reference to raw data, we plot p_0 as a function of bias phase at different pump powers (see Supplemental Material [29]). Generally, p_0 has periodic dependence on bias phase. As pumping power increases, the phase of the periodic p_0 shifts slightly. However, since we employ the phase that takes maximum (minimum) value of p_0 for positive (negative) sign of the bias field, the observed small phase shift does not affect to the shape of the sigmoid function.

In terms of application, our findings serve as a first step for potential implementation in neural networks. In this system, the shortest pulse width we can apply is 5 μs. The shortest pulse width is determined by the time required for parametric oscillation to reach steady states. For practical operation at high-frequency clock speeds, further studies will aim to reduce this pulse width by shortening the time taken for oscillations to stabilize.

In summary, we systematically investigate the dependence of the 0 and π state occurrence probability of a YIG magnetic parametron. We demonstrate its sigmoid curve behavior as a function of bias field, the steepness of which decreases with rising pump power. Our experimental result can be modeled by numerical calculation of the Wigner function of parametric oscillation under increasing dissipation.

Acknowledgments. We thank H. Shimizu for fruitful discussions. This work was partially supported by JST CREST (JPMJCR20C1 and JPMJCR20T2), JSPS KAKENHI (JP19H05600, JP22K14584, and JP22H05114), Advanced Technology Institute Research Grants 2022, and JST SPRING (JPMJSP2108).

[1] G. Cybenko, Approximation by superpositions of a sigmoidal function, Math. Control Signals Syst. **2**, 303 (1989).
[2] A. D. Jagtap, K. Kawaguchi, and G. E. Karniadakis, Adaptive activation functions accelerate convergence in deep and physics-informed neural networks, J. Comput. Phys. **404**, 109136 (2020).
[3] C. D. Schuman, S. R. Kulkarni, M. Parsa, J. P. Mitchell, P. Date, and B. Kay, Opportunities for neuromorphic computing algorithms and applications, Nat. Comput. Sci. **2**, 10 (2022).
[4] D. Christensen, R. Dittmann, B. Linares-Barranco, A. Sebastian, M. L. Gallo, A. Redaelli, S. Slesazeck, T. Mikolajick, S. Spiga, S. Menzel, I. Valov, *et al.*, 2022 roadmap on neuromorphic computing and engineering, Neuromorph. Comput. Eng. **2**, 022501 (2022).
[5] P. Kinget and M. Steyaert, A programmable analog cellular neural network CMOS chip for high speed image processing, IEEE J. Solid-State Circuits **30**, 3 (1995).
[6] A. Masaki, Y. Hirai, and M. Yamada, Neural networks in CMOS: A case study, IEEE Circuits Devices Mag. **6**, 12 (1990).
[7] A. A. Sharma, J. A. Bain, and J. A. Weldon, Phase coupling and control of oxide-based oscillators for neuromorphic computing, IEEE J. Explor. Solid-State Comput. Dev. Circuits **1**, 58 (2015).
[8] S. M. Rezende, *Fundamentals of Magnonic* (Springer Nature Switzerland AG, Cham, 2020).
[9] A. A. Serga, A. V. Chumak, and B. Hillebrands, YIG magnonics, J. Phys. D: Appl. Phys. **43**, 264002 (2010).
[10] T. Makiuchi, T. Hioki, Y. Shimazu, Y. Oikawa, N. Yokoi, S. Daimon, and E. Saitoh, Parametron on magnetic dot: Stable and stochastic operation, Appl. Phys. Lett. **118**, 022402 (2021).
[11] T. Hioki, H. Shimizu, T. Makiuchi, and E. Saitoh, State tomography for magnetization dynamics, Phys. Rev. B **104**, L100419 (2021).
[12] T. Hioki and E. Saitoh, Stochastic dynamics of a metal magnon parametron, J. Appl. Phys. **132**, 203901 (2022).
[13] M. Elyasi, E. Saitoh, and G. E. W. Bauer, Stochasticity of the magnon parametron, Phys. Rev. B **105**, 054403 (2022).
[14] T. Makiuchi, T. Hioki, H. Shimizu, K. Hoshi, M. Elyasi, K. Yamamoto, N. Yokoi, A. A. Serga, B. Hillebrands, G. E. W. Bauer, and E. Saitoh, Persistent magnetic coherence in magnets, Nat. Mater. **23**, 627 (2024).
[15] H. Shimizu, T. Hioki, and E. Saitoh, Numerical study on magnetic parametron under perpendicular excitation, Appl. Phys. Lett. **120**, 012402 (2022).
[16] D. Wei, M. Obstbaum, M. Ribow, C. H. Back, and G. Woltersdorf, Spin Hall voltages from a.c. and d.c. spin currents, Nat. Commun. **5**, 3768 (2014).
[17] C. Hahn, G. de Loubens, M. Viret, O. Klein, V. V. Naletov, and J. Ben Youssef, Detection of microwave spin pumping using the inverse spin Hall effect, Phys. Rev. Lett. **111**, 217204 (2013).
[18] H. J. Jiao and G. E. W. Bauer, Spin backflow and ac voltage generation by spin pumping and the inverse spin Hall effect, Phys. Rev. Lett. **110**, 217602 (2013).
[19] M. Weiler, J. M. Shaw, H. T. Nembach, and T. J. Silva, Phase-sensitive detection of spin pumping via the ac inverse spin Hall effect, Phys. Rev. Lett. **113**, 157204 (2014).

[20] E. Saitoh, M. Ueda, H. Miyajima, and G. Tatara, Conversion of spin current into charge current at room temperature: Inverse spin-Hall effect, Appl. Phys. Lett. **88**, 182509 (2006).

[21] A. Azevedo, L. H. Vilela Leão, R. L. Rodriguez-Suarez, A. B. Oliveira, and S. M. Rezende, Dc effect in ferromagnetic resonance: Evidence of the spin-pumping effect?, J. Appl. Phys. **97**, 10C715 (2005).

[22] T. Kimura, Y. Otani, T. Sato, S. Takahashi, and S. Maekawa, Room-temperature reversible spin Hall effect, Phys. Rev. Lett. **98**, 156601 (2007).

[23] S. O. Valenzuela and M. Tinkham, Direct electronic measurement of the spin Hall effect, Nature **442**, 176 (2006).

[24] M. V. Costache, M. Sladkov, S. M. Watts, C. H. van der Wal, and B. J. van Wees, Electrical detection of spin pumping due to the precessing magnetization of a single ferromagnet, Phys. Rev. Lett. **97**, 216603 (2006).

[25] S. Mizukami, Y. Ando, and T. Miyazaki, Effect of spin diffusion on Gilbert damping for a very thin permalloy layer in Cu/permalloy/Cu/Pt films, Phys. Rev. B **66**, 104413 (2002).

[26] Y. Kajiwara, K. Harii, S. Takahashi, J. Ohe, K. Uchida, M. Mizuguchi, H. Umezawa, H. Kawai, K. Ando, K. Takanashi, S. Maekawa, and E. Saitoh, Transmission of electrical signals by spin-wave interconversion in a magnetic insulator, Nature **464**, 262 (2010).

[27] Y. Tserkovnyak, A. Brataas, and G. E. W. Bauer, Enhanced Gilbert damping in thin ferromagnetic films, Phys. Rev. Lett. **88**, 117601 (2002).

[28] F. Guo, L. M. Belova, and R. D. McMichael, Parametric pumping of precession modes in ferromagnetic nanodisks, Phys. Rev. B **89**, 104422 (2014).

[29] See Supplemental Material at http://link.aps.org/supplemental/10.1103/PhysRevApplied.22.L031002 for detailed measurement of the microwave absorption spectrum, derivation of the Fokker-Planck equation and Wigner function, and p_0 dependence on bias phases.

[30] S. Rezende and F. de Aguiar, Spin-wave instabilities, auto-oscillations, and chaos in yttrium-iron-garnet, Proc. IEEE **78**, 893 (1990).

[31] H. Suhl, The theory of ferromagnetic resonance at high signal powers, J. Phys. Chem. Solids **1**, 209 (1957).

[32] D. Walls and G. Milburn, *Quantum Optics* (Springer-Verlag Berlin- Heidelberg, Heidelberg, 2008).

[33] H. J. Carmichael, *Statistical Method in Quantum Optics 1: Master Equations and Fokker-Planck Equations* (Springer-Verlag Berlin- Heidelberg, Heidelberg, 1999).

[34] C. W. Gardiner and P. Zoller, *Quantum Noise: A Handbook of Markovian and Non-Markovian Quantum Stochastic Methods with Applications to Quantum Optics* (Springer-Verlag Berlin- Heidelberg, Heidelberg, 2004).

[35] K. Hoshi, T. Hioki, and E. Saitoh, Spin motive force induced by parametric excitation, Appl. Phys. Lett. **121**, 212404 (2022).

[36] T. Brächer, F. Heussner, P. Pirro, T. Meyer, T. Fischer, M. Geilen, B. Heinz, B. Lägel, A. A. Serga, and B. Hillebrands, Phase-to-intensity conversion of magnonic spin currents and application to the design of a majority gate, Sci. Rep. **6**, 38235 (2016).

[37] T. Brächer, P. Pirro, and B. Hillebrands, Parallel pumping for magnon spintronics: Amplification and manipulation of magnon spin currents on the micron-scale, Phys. Rep. **699**, 1 (2017).

[38] A. A. Serga, S. O. Demokritov, B. Hillebrands, S. Min, and A. N. Slavin, Phase control of nonadiabatic parametric amplification of spin wave packets, J. Appl. Phys. **93**, 8585 (2003).

[39] G. A. Melkov, A. A. Serga, V. S. Tiberkevich, Y. V. Kobljanskij, and A. N. Slavin, Nonadiabatic interaction of a propagating wave packet with localized parametric pumping, Phys. Rev. E **63**, 066607 (2001).

[40] V. L'vov, *Wave Turbulence Under Parametric Excitation* (Springer-Verlag Berlin- Heidelberg, Heidelberg, 1994).

[41] V. E. Zakharov, V. S. L'vov, and S. S. Starobinets, Spin-wave turbulence beyond the parametric excitation threshold, Sov. Phys. Usp. **17**, 896 (1975).

[42] P. Kinsler and P. D. Drummond, Quantum dynamics of the parametric oscillator, Phys. Rev. A **43**, 6194 (1991).